Fault Detection of Broken Rotor Bars in Induction Motor Using a Global Fault Index

Gaëtan Didier, Eric Ternisien, Olivier Caspary, and Hubert Razik, *Senior Member, IEEE*

***Abstract*—Induction motors play a very important part in the safe and efficient running of any industrial plant. Early detection of abnormalities in the motor would help to avoid costly breakdowns. Accordingly, this work presents a technique for the diagnosis of broken rotor bars in induction motor. Stator voltage and current in an induction motor were measured and employed for computation of the input power of one stator phase. Waveforms of the instantaneous power and line current were subsequently analyzed using the Bartlett periodogram. Different global fault indexes on the instantaneous power spectrum and on the line current spectrum for the fault detection are evaluated. Several rotor cage faults of increasing severity were studied with various load effects. Experimental results prove the efficiency of the employed method.**

***Index Terms*—Bartlett periodogram, broken bar, diagnosis, global fault index, global modulation index, induction motor.**

I. Introduction

INDUCTION motors, especially the asynchronous motors, play an important part in the field of electromechanical energy conversion. It is well-known that interruptions of a manufacturing process due to a mechanical problem induces a serious financial loss for the firm. We know a variety of faults that can occur in induction machines [1], [2], such as rotor faults (broken bar or end ring) or rotor–stator eccentricity. In fact, if faults are undetected, they may lead to potentially catastrophic failures. The consequences of a faulty rotor are excessive vibrations, poor starting performances, torque fluctuation, or higher thermal stress.

Various techniques have been proposed to detect a rotor fault. One of the well-known approaches for the detection of broken rotor bars in an induction machine is based on the monitoring of the stator current to detect sidebands around the supply frequency [3]–[8].

Paper IPCSD-05-071, presented at the 2003 IEEE International Symposium on Diagnostics for Electrical Machines, Power Electronics and Drives, Stone Mountain, GA, August 24–26, and approved for publication in the IEEE TRANSACTIONS ON INDUSTRY APPLICATIONS by the Electric Machines Committee of the IEEE Industry Applications Society. Manuscript submitted for review March 4, 2005 and released for publication October 4, 2005. The development of the testbed was supported by the Ministère de la Recherche and by the Université Henri Poincaré of Nancy.

G. Didier and H. Razik are with the Groupe de Recherche en Electrotechnique et Electronique de Nancy, GREEN-CNRS UMR-7037, Université Henri Poincaré, Vandoeuvre-lès-Nancy Cedex 54506, France (e-mail: gaetan.didier@green.uhp-nancy.fr; hubert.razik@green.uhp-nancy.fr).

E. Ternisien and O. Caspary are with the Centre de Recherche en Automatique de Nancy, CRAN-CNRS UMR-7039, Université Henri Poincaré, Vandoeuvre-lès-Nancy Cedex 54506, France (e-mail: olivier.caspary@iutsd.uhp-nancy.fr; eric.ternisien@iutsd.uhp-nancy.fr).

Digital Object Identifier 10.1109/TIA.2005.861368

In this paper, we put forward a broken rotor bar fault detection using the power of the sidebands. The broken bar detection can be connected to the analysis of all fault components present in the line current or the instantaneous power. We estimate different global fault indexes corresponding to the contribution of all detected sidebands. We apply a nonparametric power spectrum estimation, called averaging periodograms or Bartlett method, in order to detect more precisely the frequency and the magnitude of each sideband created by the rotor fault. This method is applied on the instantaneous power of one stator phase and on its line current when the motor is connected directly to the supply voltage.

Scientists have already used the instantaneous power spectral analysis for the diagnosis of broken rotor bar. For example, in 1999, Cruz and Marques Cardoso calculated the ratio of the magnitude of the characteristic component $2sf_s$ and the dc level of the power. He showed that this severity factor is independent of motor rating and motor-load inertia [9]. In 1996 and 2000, Legowski *et al.* [10] and Trzynadlowski and Ritchie [11] compared the partial and total instantaneous power to the line current and concluded that the latter yields inferior results to the first for broken rotor bars detection and mechanical abnormalities in induction motor.

The advantages of the use of the instantaneous power spectrum are given as follows:

1) presence of additional components in low frequencies;
2) first low-frequency component is positioned directly at the speed oscillation frequency;
3) easier filtering of the dc component in the power spectrum than to remove the 50-Hz fundamental component in the current spectrum without affecting the components at $(1 \pm 2s)f_s$ in case of a very little slip (s represents the slip of the machine and f_s the supply frequency).

The method exposed in this paper, in comparison to the works quoted previously, uses all components created by the rotor fault in the instantaneous power spectrum for the final diagnosis. We show that additional information carried by the instantaneous power in low frequency improves the diagnosis of broken rotor bars. In fact, such an instantaneous power method can be interpreted as a modulation operation in the time domain that translates the spectral components specific to the broken rotor bar to a well-bounded 0–50-Hz frequency [12]–[14]. We show that the diagnosis of a partially broken rotor bar ($\simeq$ half broken bar) can be carried out even if the motor operates under low load.

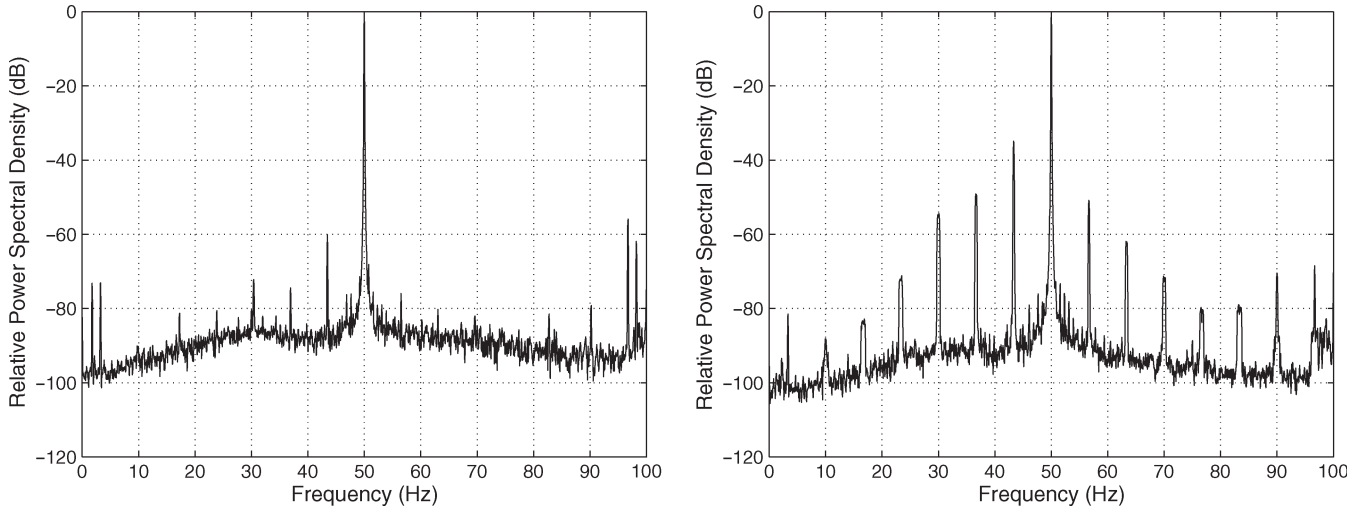

Fig. 1. Current spectrum for (a) a healthy rotor and (b) one broken rotor bar.

II. Instantaneous Power Signature

First, we consider an ideal three-phase supply voltage. The instantaneous power $p_s(t)$ of one phase is classically given by

$$p_s(t) = v_s(t) i_s(t) \tag{1}$$

where $v_s(t)$ is the instantaneous line voltage and $i_s(t)$ stands as its line current. If those two conditions are respected, the supply voltage is sinusoidal and the speed is constant (no ripple). The instantaneous power can be written as

$$v_s(t) = \sqrt{2} V_s \cos(\omega t) \tag{2}$$

$$i_{s0}(t) = \sqrt{2} I_s \cos(\omega t - \varphi) \tag{3}$$

$$p_{s0}(t) = V_s I_s \left[\cos(2\omega t - \varphi) + \cos\varphi\right] \tag{4}$$

where φ is the phase angle between the voltage and the current line. The power spectrum of the current has only one fundamental component at the frequency $f_s = \omega/(2\pi)$, while the instantaneous power spectrum has a dc component and its fundamental component at the frequency $2f_s = (2\omega)/(2\pi)$.

When a bar breaks, a rotor asymmetry occurs. The result is the appearance of a backward-rotating field at the slip frequency sf_s with respect to the forward-rotating rotor. It induces in the stator current an additional frequency at $f_{bb_{ls}} = (1-2s)f_s$. This cyclic current variation implies a speed oscillation and a torque pulsation at the twice slip frequency $(2sf_s)$. This speed oscillation induces, in the stator winding, an upper component at $f_{bb_{hs}} = (1+2s)f_s$. Briefly, broken rotor bars induce in the stator winding additional components at frequencies given by

$$f_{bb_s} = (1 \pm 2ks) f_s \tag{5}$$

where $k = 1, 2, 3, \ldots$.

Therefore, the current is modulated and can be written as [13]

$$i_s(t) = i_{s0}(t)\left[1 + \sum_h M_{c_h} \cos(h\omega_f t)\right] \tag{6}$$

$$i_s(t) = i_{s0}(t) + \sum_h \frac{\sqrt{2} M_{c_h} I_s}{2} \times \left[\cos\left((\omega - h\omega_f)t - \varphi\right) + \cos\left((\omega + h\omega_f)t - \varphi\right)\right] \tag{7}$$

where M_{c_h} denotes the modulation depth (modulation index) and $h = 1, 2, 3, \ldots$.

The last expression considers that the magnitude of the left and the right components are identical for the same index h. If we take a look at Fig. 1(a) and (b), which represents the line current spectrum with a healthy rotor and one broken bar, we can see that the components at $f_{bb_s} = (1-2ks)f_s$ do not have the same magnitude as the components at $f_{bb_s} = (1+2ks)f_s$ for the same index h (influence of the load inertia). Consequently, we have to separate the magnitude of the left and the right components in (7) by introducing an index for each component [this index is called magnitude index to make a distinction with the modulation index presents in (6)]. The new expression of the modulated current is given by

$$i_s(t) = i_{s0}(t) + \sum_k \frac{\sqrt{2} M_{c_k} I_s}{2} \cos\left((\omega - k\omega_f)t - \varphi\right) + \sum_k \frac{\sqrt{2} M'_{c_k} I_s}{2} \cos\left((\omega + k\omega_f)t - \varphi\right) \tag{8}$$

where M_{c_k} denotes the magnitude index for the left components, M'_{c_k} denotes the magnitude index for the right components, and $f_f = w_f/2\pi = 2sf_s$ acts as the modulation

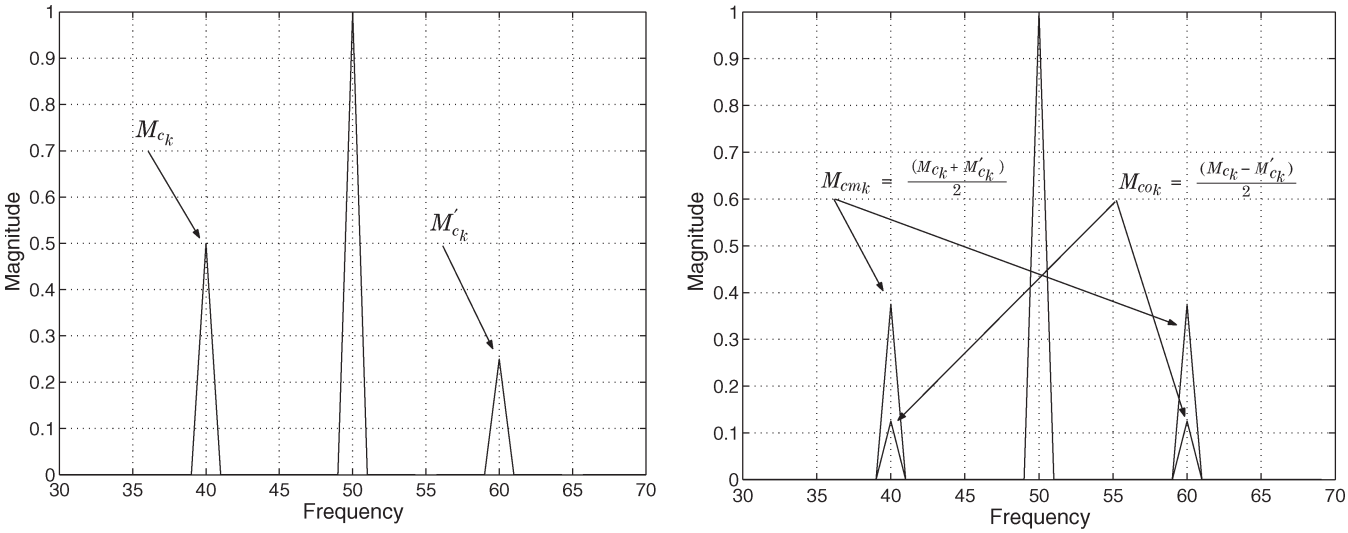

(a) (b)

Fig. 2. (a) Magnitude indexes of the left and right components, (b) modulation index M_{cm_k}, and (c) oscillation index M_{co_k}.

frequency. If we develop the cosine terms, we can put this last expression in the form

$$\begin{aligned} i_s(t) = i_{s0}(t) &+ \sum_k \frac{\sqrt{2}I_s}{2}\left(M_{c_k} + M'_{c_k}\right)\cos(k\omega_f t) \\ &\times \left(\cos\varphi\cos(\omega t) + \sin\varphi\sin(\omega t)\right) \\ &+ \sum_k \frac{\sqrt{2}I_s}{2}\left(M_{c_k} - M'_{c_k}\right)\sin(k\omega_f t) \\ &\times \left(\cos\varphi\sin(\omega t) - \sin\varphi\cos(\omega t)\right). \end{aligned} \tag{9}$$

This expression allows us to find a similarity with (6) given previously. We can see in (9) that, if we consider only the study of the magnitude, we define two new indexes as

$$M_{cm_k} = \frac{\left(M_{c_k} + M'_{c_k}\right)}{2} \tag{10}$$

$$M_{co_k} = \frac{\left(M_{c_k} - M'_{c_k}\right)}{2}. \tag{11}$$

The first corresponds to the modulation index usually used in the signal theory, and the second will be called as oscillation index in this paper. Fig. 2(a) and (b) shows us a theoretical spectrum to explain the origin of the different indexes used in (8) and (9).

The mathematical expression for the modulated instantaneous power of one phase is obtained by multiplying (2) by (8) and is written as

$$\begin{aligned} p_s(t) = p_{s0}(t) &+ \sum_k \frac{M_{p_k}V_sI_s}{2}\cos\left((2\omega - k\omega_f)t - \varphi\right) \\ &+ \sum_k \frac{M'_{p_k}V_sI_s}{2}\cos\left((2\omega + k\omega_f)t - \varphi\right) \\ &+ \sum_k \frac{V_sI_s}{2}\left[M_{p_k} + M'_{p_k}\right]\cos\varphi\cos(kw_f t) \\ &+ \sum_k \frac{V_sI_s}{2}\left[M'_{p_k} - M_{p_k}\right]\sin\varphi\sin(kw_f t). \end{aligned} \tag{12}$$

In addition to the fundamental frequency and sideband components at $f = (2\omega \pm \omega_f)/(2\pi)$ for the case of $k = 1$, we have a spectral peak at the modulation frequency $f_f = \omega_f/(2\pi)$ in the instantaneous power spectrum. The latter, referred to the characteristic component, provides an additional indication of diagnosis information about the state of the motor. Its amplitude depends on phase angle φ and on indexes M_{p_1} and M'_{p_1}. In our case, this component is used for the calculation of the $2sf_s$ frequency. This value could be used for the induction machine speed estimation. If we rewrite (12) in the same form as (9), we obtain for the expression of the modulation index M_{pm_k} and for the oscillation index M_{po_k} of the instantaneous power the expressions

$$M_{pm_k} = \frac{\left(M_{p_k} + M'_{p_k}\right)}{2} \tag{13}$$

$$M_{po_k} = \frac{\left(M_{p_k} - M'_{p_k}\right)}{2}. \tag{14}$$

The value of magnitude indexes M_{c_k}, M'_{c_k}, M_{p_k}, and M'_{p_k} depends on the severity of the abnormality. In fact, these indexes will increase when a broken bar appears, because magnitudes of the different components created by the rotor fault will increase. We could use this information for the broken rotor bars diagnosis of induction motor.

III. Broken Bar Detection Based on the Global Fault Index

In the case of a healthy motor, the equation of the instantaneous power contains an amplitude modulation with one modulation signal around the carrier frequency at 100 Hz. In fact, this modulation signal is created by a natural rotor asymmetry (eccentricity created by the load for example). If a broken rotor bar occurs, this asymmetry increases, and several sidebands appear at the modulation frequency $2ksf_s$. According to the amplitude modulation theory, if several sinusoidal signals modulate the same carrier wave, the power of this wave

does not change while the modulating signals increase the power contained in sidebands. Since the modulation index is proportional to the amplitude of the modulating signal, different modulation indexes correspond to different modulating signals. The global modulation index M_{gm_x} is defined such that the power of sidebands equals the sum of powers of each sideband

$$\frac{M_{gm_x}^2 P_c}{2} = \sum_k \frac{M_{xm_k}^2 P_c}{2} \tag{15}$$

where the spectral power P_c of the carrier frequency is $P_c = (V_s I_s)^2$ with the signal $p_s(t)$. The subscript letter x in the latter expression can be replaced by p (instantaneous power) or c (line current). For the global oscillation index M_{go_x}, we have

$$\frac{M_{go_x}^2 P_c}{2} = \sum_k \frac{M_{xo_k}^2 P_c}{2}. \tag{16}$$

If we have a look at (8) and (12), we propose to calculate a new index, which we call global fault index M_{t_x}, with the expression

$$\frac{M_{t_x}^2 P_c}{2} = \sum_k \frac{M_{x_k}^2 P_c}{2} + \sum_k \frac{M_{x_k}'^2 P_c}{2}. \tag{17}$$

This expression was chosen so as to find a similarity with the signal theory. The expression of M_{t_x}, by supposing K_l as the number of components at the left of the supply frequency and K_r as the number of components at the right, becomes

$$M_{t_x}^2 = \sum_{k=1}^{K_l} M_{x_k}^2 + \sum_{k=1}^{K_r} M_{x_k}'^2. \tag{18}$$

Moreover, for each modulation frequency $(2f_s \pm 2ksf_s)$ for the instantaneous power spectrum and $(f_s \pm 2ksf_s)$ for the line current spectrum, we can deduce its magnitude index M_z by dividing its estimated amplitude $A_{s_z} = M_z A_c/2$ by the amplitude of the carrier frequency $A_c = V_s I_s$ (z can be replaced by c_k for the line current and p_k for the instantaneous power) as

$$\frac{A_{s_z}}{A_c} = \frac{M_z A_c}{2}\frac{1}{A_c} = \frac{M_z}{2}$$

$$M_z = \frac{2A_{s_z}}{A_c}. \tag{19}$$

The same method can be applied for the low-frequency components of the instantaneous power. In fact, we have seen previously that instantaneous power spectrum contains additional components in low frequency. We can use the magnitude of these components to determine their global fault index. With (12), we can give the mathematical relation of the low-frequency component's magnitude for a specific value of k as

$$A_{p_k} = \sum_k \frac{V_s I_s}{2}\sqrt{M_{p_k}^2 + M_{p_k}'^2 + 2M_{p_k}M_{p_k}'\cos(2\varphi)} \tag{20}$$

where A_{pk} denotes the magnitude of the low-frequency component k present in the instantaneous power spectrum. With the latter expression, we can deduce a new fault index M_{lf_k} specific to those components as

$$M_{lf_k} = \sqrt{M_{p_k}^2 + M_{p_k}'^2 + 2M_{p_k}M_{p_k}'\cos(2\varphi)} \tag{21}$$

and, consequently, we can deduce the global fault index for the low-frequency components with the expression

$$M_{t_{lf}}^2 = \sum_{k=1}^{K_{pn}} M_{lf_k}^2 \tag{22}$$

where K_{pn} represents the number of components detected in the low-frequency band.

Thus, the broken bar detection can be connected to the analysis of the global modulation index M_{gm_x}, the global oscillation index M_{go_x}, the global fault index M_{t_x}, and the low-frequency global fault index $M_{t_{lf}}$. If a fault appears in the rotor cage, we will have an increase of those global indexes and, consequently, a good indication for the diagnosis of the motor. To evaluate those global indexes, we must find the frequency and amplitude of each sideband to estimate the magnitude indexes M_{x_k}, M_{x_k}', and M_{lf_k}.

To reduce the variance in the spectrum and to improve the evaluation of the component's magnitude, we apply a nonparametric power spectrum estimation, called averaging periodograms or Bartlett method, instead of the classic periodogram [15]. Indeed, when the record length N increases, the frequency resolution of the periodogram is better, but its variance is not reduced. The definition of the periodogram is written as

$$\hat{P}_{p_s}(f) = \frac{1}{N}\left|\sum_{m=0}^{N-1}\omega(m)p_s(m)e^{-j2\pi fm}\right|^2 \tag{23}$$

and it can be calculated from a discrete Fourier transform (DFT) or a fast Fourier transform (FFT). We can use a window $\omega(m)$ if necessary to form the modified periodogram. For the Bartlett periodogram, the data sequence of N samples is divided into L nonoverlapping segments of D samples such as $DL < N$. The modified periodograms of each segment are averaged in order to reduce the variance of the Bartlett periodogram as [16]

$$\hat{P}_{p_s}^B(f) = \frac{1}{L}\sum_{i=0}^{L-1}\hat{P}_{p_s}^{(i)}(f) \tag{24}$$

where $\hat{P}_{p_s}^{(i)}(f)$ is the modified periodogram of the ith segment of the signal $p_s(m)$. Overlapped segments can be used to form the Welch periodogram, but it is not necessary in our case because of the high number of samples.

Nevertheless, the Bartlett periodogram is only fitted for the use with an operation at steady state as it is the case in this study.

IV. Experimental Results

The testbed used in the experimental investigation is composed of a three-phase induction motor, 50 Hz, two poles, and 3 kW [Fig. 3(a)]. In order to test the effectiveness of the

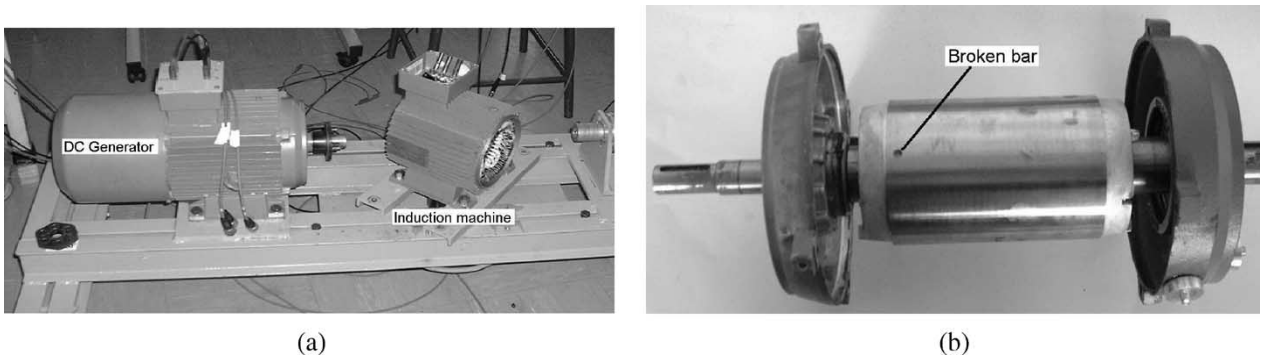

Fig. 3. (a) Testbed and (b) position of the broken rotor bar.

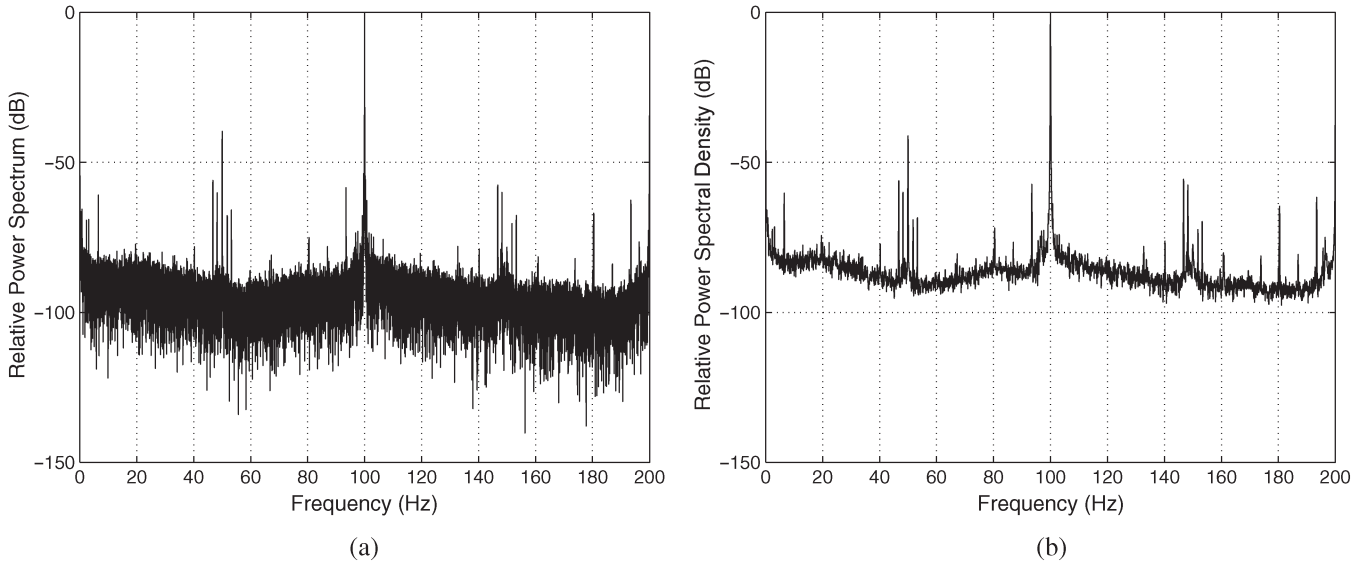

Fig. 4. (a) Classic periodogram and (b) Bartlett periodogram of $p_s(t)$ for the healthy rotor.

suggested method, we have several identical rotors with 28 bars, which can be exchanged without affecting the electrical and magnetic features. The position of the broken bar is given in Fig. 3(b). The voltage and the line current measurements were made at the nominal rate. For those two variables, the sampling frequency was 2 kHz, and each data length was equal to 2^{18} values.

We can see in Fig. 4(a) and (b), which represents the power spectrum of the instantaneous power of one phase for the healthy rotor (referred to the 100-Hz fundamental), that the noise level is reduced thanks to the averaging by using the Bartlett periodogram (the data length D for the average is equal to 2^{15} values). We have shown in [17] that the use of a Hanning's window for the calculation of the Bartlett periodogram [$\omega(m)$ in (23)] improves the detection of the component's magnitude for the evaluation of magnitude indexes M_{c_k}, M'_{c_k}, M_{p_k}, and M'_{p_k}.

We keep a good estimation of the sidebands' power translated from 0 Hz by avoiding numerous maxima peaks contained in each one because of a very slight frequency variation of the slip. Consequently, we can consider the detection of maxima peaks in the spectrum. The first frequency that we want to detect is the $2sf_s$ frequency, because it corresponds to the component with the highest power that is not disrupted by the supply power when we remove the mean of the instantaneous power signal. Then, we search all maxima from this first frequency, which are at frequencies $2ksf_s$ in the considered 1–35-Hz band with a greater accuracy (the tolerance is below 1%) and above a threshold defined as the mean of this spectral band. This information gives us the number of components K_{pn} and the magnitude of each one. With those magnitudes, we can calculate the global modulation index M_{lf_k} specific to the low-frequency components with (22). The value K_{pn}, multiplied by two, gives us the total number of components that we must detect on both sides of the carrier frequency of $p_s(t)$ and $i_s(t)$. We calculate the frequencies $2(1 \pm ks)f_s$ in the instantaneous power spectrum and $(1 \pm 2ks)f_s$ in the current spectrum to evaluate their magnitudes. Then, we estimate the magnitude index of each modulation frequency in the same way as (19). In the end, with (15), (16), (18), and (22), we can calculate the global modulation index M_{gm_c}, the oscillation index M_{go_c}, and the global fault index M_{t_c} specific to the line current spectrum and the global modulation index M_{gm_p}, the oscillation index M_{go_p}, the global fault index M_{t_p}, and the low-frequency global fault index $M_{t_{lf}}$ specific to the instantaneous power spectrum. We made a comparison between those seven various indexes in the continuation of the paper to find which is the most judicious to base the diagnosis of broken rotor bars.

TABLE I
CALCULATION OF DIFFERENT GLOBAL INDEXES

Motor	$2sf_s$ frequency	Speed (r/min)	K_{pn}	$M_{t_{lf}}$	M_{t_p}	M_{t_c}	M_{gm_p}	M_{go_p}	M_{gm_c}	M_{go_c}
H-L100	6.53	2804	2	0.0020	0.0028	0.0021	0.0015	0.0012	0.0012	0.0009
05b-L100	5.98	2820	3	0.0063	0.0060	0.0058	0.0037	0.0021	0.0033	0.0018
1b-L100	6.67	2799	3	0.0435	0.0454	0.0408	0.0260	0.0189	0.0237	0.0164
H-L75	4.94	2851	3	0.0024	0.0036	0.0024	0.0021	0.0015	0.0014	0.0008
05b-L75	4.27	2871	3	0.0057	0.0064	0.0051	0.0040	0.0021	0.0032	0.0015
1b-L75	4.64	2860	4	0.0408	0.0470	0.0442	0.0288	0.0165	0.0274	0.0151
H-L50	3.17	2904	2	0.0017	0.0023	0.0018	0.0015	0.0007	0.0012	0.0004
05b-L50	2.87	2913	3	0.0040	0.0057	0.0038	0.0037	0.0017	0.0026	0.0007
1b-L50	2.99	2910	4	0.0279	0.0393	0.0350	0.0256	0.0109	0.0233	0.0083
H-L25	1.59	2952	2	0.0044	0.0100	0.0048	0.0059	0.0038	0.0030	0.0014
05b-L25	1.47	2956	2	0.0115	0.0214	0.0100	0.0120	0.0092	0.0061	0.0036
1b-L25	1.53	2954	3	0.0240	0.0358	0.0281	0.0246	0.0059	0.0198	0.0019

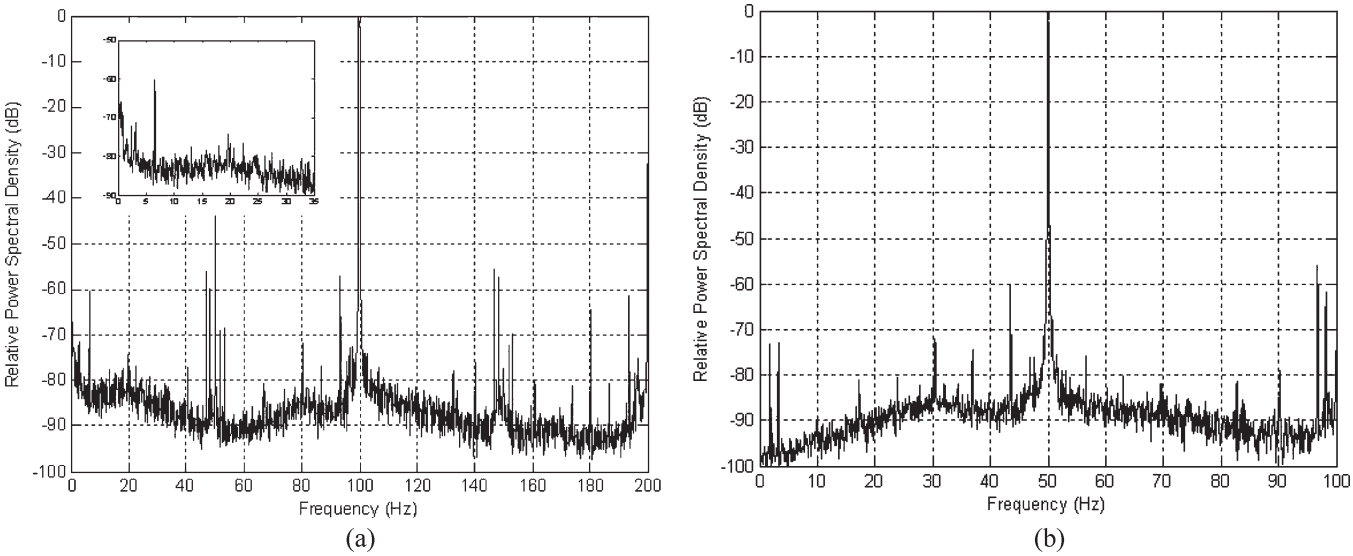

Fig. 5. (a) Bartlett periodogram of instantaneous power and (b) line current for a healthy rotor (100% load).

We studied the case of a partially broken rotor bar and one broken rotor bar with different load levels. Table I shows the results obtained by the proposed method. In this table, we report the state of the motor (for example, we note H-L100, the case of a healthy rotor with 100% load, and 05b-L25, the case of a partially broken rotor bar with 25% load), the value of the $2sf_s$ frequency, the speed of the motor, the number of peaks K_{pn} found in the 1–35-Hz band, the value of the three different global fault indexes, the value of the two different global modulation indexes, and, finally, the value of the two different global oscillation indexes.

Fig. 5(a) and (b) represents the line current and the instantaneous power spectra for a healthy rotor. We can note that instantaneous power spectrum contains a modulation frequency at $2sf_s$ (which is induced by a natural eccentricity of the rotor) and a component at the frequency $2(1-s)f_s$. This component is also present in the line current spectrum at the frequency $(1-2s)f_s$. The same phenomenon appears in Fig. 6(a) and (b) for the 25% load. This modulation frequency allows the calculus of global indexes in the case of a healthy rotor. Those indexes will stand as a reference for the broken rotor bar diagnosis.

We can see in Fig. 7(a) and (b) for the 100% load and Fig. 8(a) and (b) for the 25% load that when a rotor fault appears, the components created by the asymmetry increase in magnitude in the line current and instantaneous power spectra. We see in Table I that, in the case of one broken rotor bar, global fault indexes, global modulation indexes, and global oscillation indexes increase in a very significant way. For a partially broken rotor bar, these indexes increase but with a less significant value than for the test with one broken rotor bar. Moreover, Table I shows us that the number of peaks K_{pn} detected in the low-frequency band of the instantaneous power spectrum also increases with the rotor fault.

Consequently, for the broken rotor bar diagnosis, we established a criterion that takes into account global indexes (modulation, oscillation, and fault) and the number of peaks K_{pn}. This criterion is given in Table II. Index M_X represents one of the seven global indexes (M_{gm_p}, M_{go_p}, M_{gm_c}, M_{go_c}, $M_{t_{lf}}$, M_{t_p}, or M_{t_c}). The term α is called index of sensitivity and takes a value of 2 in this case ($\alpha = 2$).

Table III gives us the results of the criterion explained previously applied to the three global fault indexes. The last column is composed of the colors green, orange, and red as

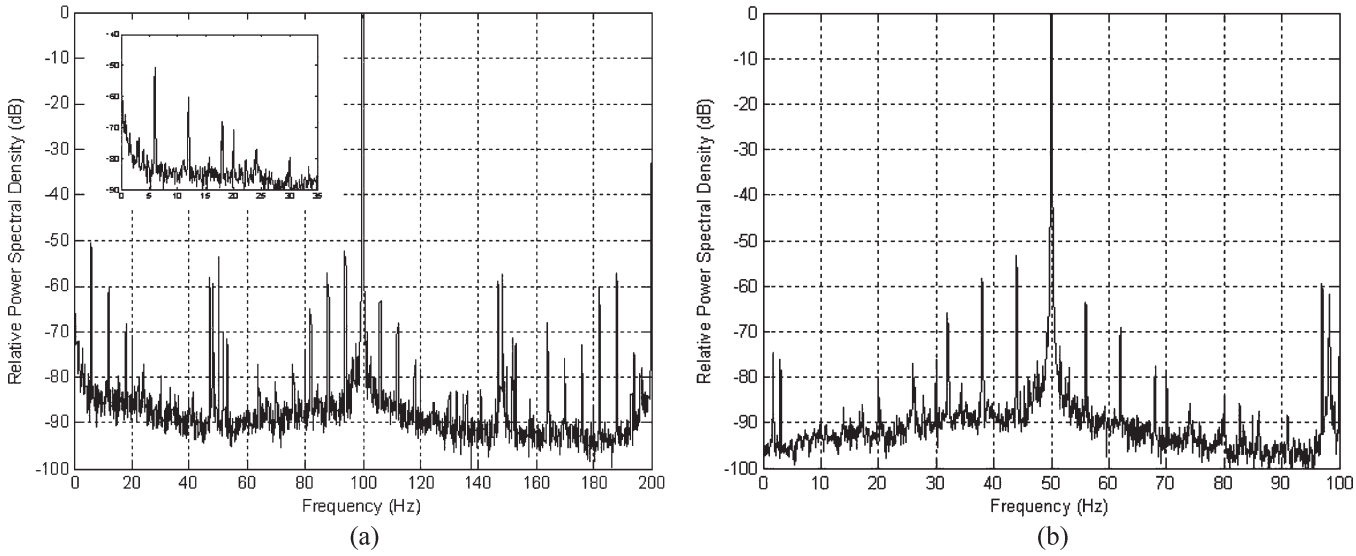

Fig. 6. (a) Bartlett periodogram of instantaneous power and (b) line current for a healthy rotor (25% load).

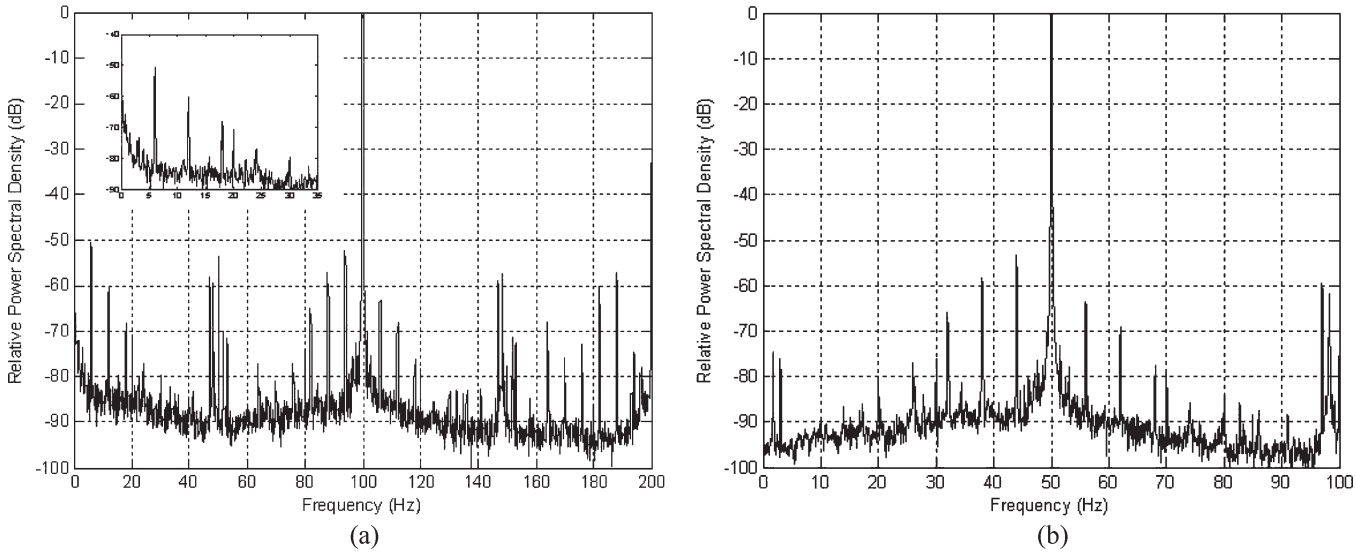

Fig. 7. (a) Bartlett periodogram of instantaneous power and (b) line current for a partially broken bar (100% load).

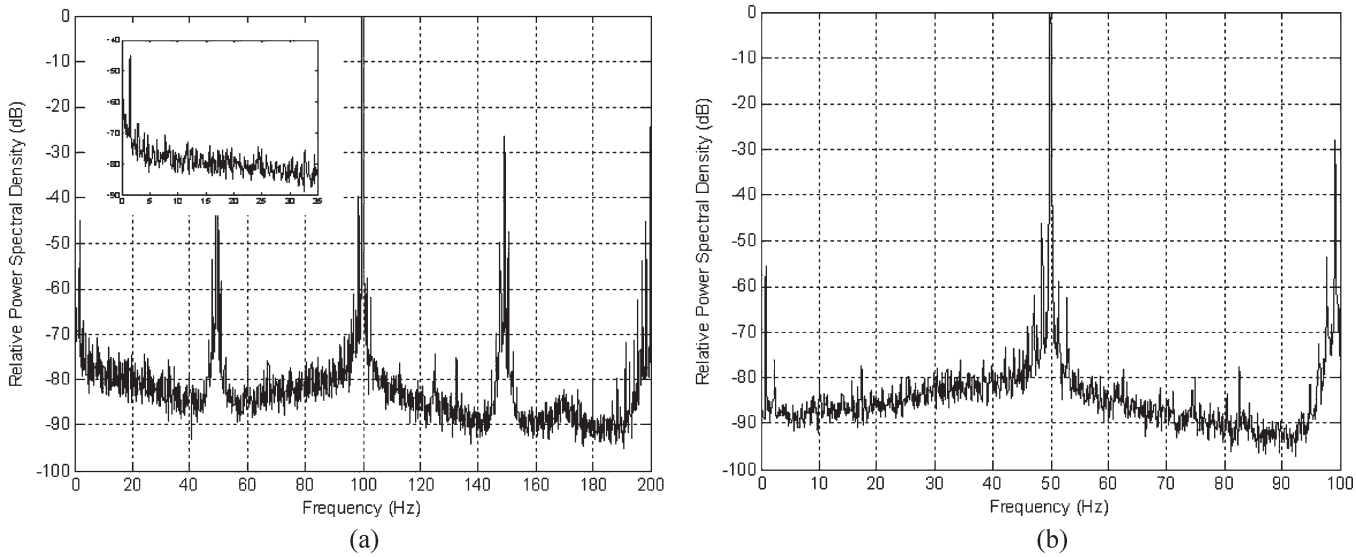

Fig. 8. (a) Bartlett periodogram of instantaneous power and (b) line current for a partially broken bar (25% load).

TABLE II
CRITERION USED FOR THE FAULT DETECTION

Test	Result
$if\ (M_{X_{Measured}} < \alpha M_{X_{Healthy}})$	No fault (Green color)
$if\ (M_{X_{Measured}} \geq \alpha M_{X_{Healthy}})\ \&\ (K_{pn_{Measured}} = K_{pn_{Healthy}})$	Incipient rotor fault (Orange color)
$if\ (M_{X_{Measured}} \geq \alpha M_{X_{Healthy}})\ \&\ (K_{pn_{Measured}} > K_{pn_{Healthy}})$	Rotor Fault (Red color)

TABLE III
COMPARISON BETWEEN DIFFERENT GLOBAL FAULT INDEXES

Motor	K_{pn}	M_{gm_p}	αM_{gm_p}	C	M_{go_p}	αM_{go_p}	C	M_{gm_c}	αM_{gm_c}	C	M_{go_c}	αM_{go_c}	C
H-L100	2	0.0015	0.0030	G	0.0012	0.0024	G	0.0012	0.0024	G	0.0009	0.0018	G
05b-L100	3	0.0037	0.0030	R	0.0021	0.0024	**G**	0.0033	0.0024	R	0.0018	0.0018	R
1b-L100	3	0.0260	0.0030	R	0.0189	0.0024	R	0.0237	0.0024	R	0.0164	0.0018	R
H-L75	3	0.0021	0.0042	G	0.0015	0.0030	G	0.0014	0.0028	G	0.0008	0.0016	G
05b-L75	3	0.0040	0.0042	**G**	0.0021	0.0030	**G**	0.0032	0.0028	O	0.0015	0.0016	**G**
1b-L75	4	0.0288	0.0042	R	0.0165	0.0030	R	0.0274	0.0028	R	0.0151	0.0016	R
H-L50	2	0.0015	0.0030	G	0.0007	0.0014	G	0.0012	0.0024	G	0.0004	0.0008	G
05b-L50	3	0.0037	0.0030	R	0.0017	0.0014	R	0.0026	0.0024	R	0.0007	0.0008	**G**
1b-L50	4	0.0256	0.0030	R	0.0109	0.0014	R	0.0233	0.0024	R	0.0083	0.0008	R
H-L25	2	0.0059	0.0118	G	0.0038	0.0076	G	0.0030	0.0060	G	0.0014	0.0028	G
05b-L25	2	0.0120	0.0118	O	0.0092	0.0076	O	0.0061	0.0060	O	0.0036	0.0028	O
1b-L25	3	0.0246	0.0118	R	0.0059	0.0076	**G**	0.0198	0.0060	R	0.0019	0.0028	**G**

TABLE IV
COMPARISON BETWEEN DIFFERENT GLOBAL MODULATION INDEXES AND GLOBAL OSCILLATION INDEXES

Motor	K_{pn}	$M_{t_{lf}}$	$\alpha M_{t_{lf}}$	Color	M_{t_p}	αM_{t_p}	Color	M_{t_c}	αM_{t_c}	Color
H-L100	2	0.0020	0.0040	G	0.0028	0.0056	G	0.0021	0.0042	G
05b-L100	3	0.0063	0.0040	R	0.0060	0.0056	R	0.0058	0.0042	R
1b-L100	3	0.0435	0.0040	R	0.0454	0.0056	R	0.0408	0.0042	R
H-L75	3	0.0024	0.0048	G	0.0036	0.0072	G	0.0024	0.0048	G
05b-L75	3	0.0057	0.0048	O	0.0064	0.0072	**G**	0.0051	0.0048	O
1b-L75	4	0.0408	0.0048	R	0.0470	0.0072	R	0.0442	0.0048	R
H-L50	2	0.0017	0.0034	G	0.0023	0.0046	G	0.0018	0.0036	G
05b-L50	3	0.0040	0.0034	R	0.0057	0.0046	R	0.0038	0.0036	R
1b-L50	4	0.0279	0.0034	R	0.0393	0.0046	R	0.0350	0.0036	R
H-L25	2	0.0044	0.0088	G	0.0100	0.0200	G	0.0048	0.0096	G
05b-L25	2	0.0115	0.0088	O	0.0214	0.0200	O	0.0100	0.0096	O
1b-L25	3	0.0240	0.0088	R	0.0358	0.0200	R	0.0281	0.0096	R

previously mentioned. With the use of the global fault index M_{t_p}, the criterion does not detect the incipient rotor fault (partially broken rotor bar) with 75% load. With global fault indexes $M_{t_{lf}}$ and M_{t_c}, the detection of rotor faults is possible in all cases. If we take a look at Table IV, which gives the results of the criterion applied to global modulation indexes and to global oscillation indexes, we can deduce that only the global modulation M_{gm_c} allows the detection of all faults. Global index M_{gm_p} does not detect a partially broken rotor bar with 75% load. In the case of the global index M_{go_p}, it is a partially broken rotor bar with 75% and 100% loads and one broken rotor bar with 25% load, which are not detected. Moreover, if we refer to global oscillation index M_{go_c}, it is a partially broken rotor bar with 50% and 75% loads and one broken rotor bar with 25% load, which are not detected.

According to the latter notes, only the low-frequency global fault index of the instantaneous power $M_{t_{lf}}$, the global fault index M_{t_c}, and the global modulation index M_{gm_c} of the line current allow the detection of all faults. Table V shows the increase of those three global fault indexes for each defect. We can deduce that the global fault index specific to the low frequency of the instantaneous power spectrum $M_{t_{lf}}$ allows a detection of the partially broken rotor bar faster than global fault indexes of the line current M_{t_c} and M_{gm_c}, because it increases more significantly.

TABLE V
INCREASE OF GLOBAL FAULT INDEXES $M_{t_{lf}}$, M_{t_c}, AND M_{gm_c}

Motor	$M_{t_{lf}}$	M_{t_c}	M_{gm_c}
05b-L100	215 %	176 %	175 %
1b-L100	2075 %	1842 %	1875 %
05b-L75	137 %	112 %	128 %
1b-L75	1600 %	1741 %	1857 %
05b-L50	135 %	111 %	116 %
1b-L50	1541 %	1844 %	1841 %
05b-L25	161 %	108 %	103 %
1b-L25	445 %	485 %	560 %

Consequently, we advocate the use of the global fault index $M_{t_{lf}}$ specific to the low-frequency components of the instantaneous power of one stator phase for the broken rotor bar diagnosis in induction motor. Besides, with the exposed method, an incipient rotor fault generated by a partially broken rotor bar in the rotor cage with 25% load has been detected. With a load inferior to 25%, the broken rotor bar detection remains difficult with this method, because the instantaneous power of the motor is absorbed by the stator (stator ohmic losses and stator core losses). The power transmitted to the rotor is

very low. However, if we consider the fact that, in industrial applications, the motors operate with a load level higher than 50%, the presented method gives very good information about the state of the rotor cage.

If we make a comparison to other techniques such as pattern recognition [18] or neural network ones, this approach presents some advantages. First, our method does not need a training to create a classifier (only a few tests with a healthy rotor at a specific load are needed). Consequently, it is not necessary to make a lot of tests to obtain training samples. Moreover, the method allows the detection of an incipient rotor fault (0.5/28 bars). This point may be difficult since the two classes (healthy and half broken bar) are very close to each other, and decision is difficult to take. Finally, if we consider the case of a digital signal processing (DSP) implementation, the computational time is faster (only an FFT calculus and a few operations).

V. Conclusion

In this paper, a novel approach of diagnosis on induction motor has been put forward and tested. The diagnosis based on the global fault index method applied to the instantaneous power signal and line current signal provides relevant results for the detection of broken rotor bars. A comparison between those two signals allowed to show that the detection of a partially broken rotor bar is faster if we use the low-frequency global fault index of the instantaneous power. We have demonstrated that a half broken bar with 25% load can be detected using the criterion that has been developed previously. The experimental results showed up the effectiveness of the technique, even if the motor operates under a low load.

We can note that this method can be used for the detection of mechanical faults (for example, pulsation torque at the twice slip frequency). In this case, the components present around the supply frequency of the line current and instantaneous power have the same frequencies with the components created by a broken rotor bar fault. In addition to the components present around the supply frequency, it is well known that rotor cage fault creates additional components at frequencies $((k/p)(1-s) \pm s)f_s$, where k/p denotes the space harmonic number $(3, 5, 7, \ldots)$ [19]. The evaluation of a new global fault index, specific to the components present near space harmonics, could be done. In fact, we know that when a mechanical fault appears, contrary to a rotor fault, those components are not disrupted. Indeed, a broken rotor bar induces a modification of the rotor induction (fundamental and space harmonics), which results in an increase of the component's harmonics amplitude in the line current spectrum. This phenomenon does not appear in the case for a load torque variation. With this study, we could differentiate a mechanical fault from a rotor fault with good accuracy [20].

The method can also be extended to the detection of eccentricity faults. A new fault index, specific to static and/or dynamic eccentricities can be created by monitoring components situated at frequencies [21]

$$f_{sh} = \left[(kR \pm n_d)\frac{(1-s)}{p} \pm v \right] f_s \qquad (25)$$

where $k = 0, 1, 2, \ldots$, R is the number of rotor slots, n_d is known as eccentricity order, and $v = \pm 1, \pm 3, \ldots$ is the order of stator time harmonics that are present in the power supply. If the index increases with regards to the healthy rotor reference, an eccentricity fault is detected.

Finally, in order to make α independent of machine parameters, additional tests with different motors will be necessary.

Appendix
Parameters of Motor Used in Experiments

Number of poles	2;
rated power	3 kW;
rated voltage	230 V;
rated current	5.90 A;
rated frequency	50 Hz;
rated speed	2800 r/min;
number of stator slots	36;
number of rotor bars	28.

References

[1] A. H. Bonnet, "Analysis of rotor failures in squirrel cage induction machines," *IEEE Trans. Ind. Appl.*, vol. 24, no. 6, pp. 1124–1130, Nov./Dec. 1988.

[2] A. H. Bonnet and G. C. Soukup, "Cause and analysis of stator and rotor failures in three-phase squirrel-cage induction motors," *IEEE Trans. Ind. Appl.*, vol. 28, no. 4, pp. 921–937, Jul./Aug. 1992.

[3] S. Nandi and H. A. Toliyat, "Fault diagnosis of electrical machine—A review," in *Proc. Int. Electric Machines and Drives Conf. (IEMDC)*, Seattle, WA, May 1999, pp. 219–221.

[4] W. T. Thomson and M. Fenger, "Current signature analysis to detect induction motor faults," *IEEE Ind. Appl. Mag.*, vol. 7, no. 4, pp. 26–34, Jul./Aug. 2001.

[5] G. B. Kliman and J. Stein, "Induction motor fault detection via passive current monitoring," in *Proc. Int. Conf. Electrical Machines (ICEM)*, Cambridge, MA, 1990, vol. 1, pp. 13–17.

[6] G. B. Kliman, J. Stein, R. D. Endicott, and R. A. Koegl, "Noninvasive detection of broken rotor bars in operating induction motor," *IEEE Trans. Energy Convers.*, vol. 3, no. 4, pp. 873–879, Dec. 1998.

[7] G. Didier, H. Razik, and A. Rezzoug, "On the modelling of induction motor including the first space harmonics for diagnosis purposes," in *Proc. Int. Conf. Electrical Machine (ICEM)*, Bruges, Belgium, Aug. 2002, CD-ROM.

[8] G. Didier, H. Razik, A. Abed, and A. Rezzoug, "On space harmonics model of a three phase squirrel cage induction motor for diagnosis purposes," in *Proc. Int. Eur. Power Electronics-Power Electronics and Motion Control (EPE-PEMC) Conf.*, Cavtat & Dubrovnik, Croatia, Sep. 2002, CD-ROM.

[9] S. M. A. Cruz and A. J. Marques Cardoso, "Rotor cage fault diagnosis in three phase induction motors by the total instantaneous power spectral analysis," in *Conf. Rec. IEEE-IAS Annu. Meeting*, Phoenix, AZ, Oct. 3–7, 1999, vol. 3, pp. 1929–1934.

[10] S. F. Legowski, A. H. M. Sadrul Ula, and A. M. Trzynadlowski, "Instantaneous power as a medium for the signature analysis of induction motors," *IEEE Trans. Ind. Electron.*, vol. 47, no. 5, pp. 984–993, Oct. 1996.

[11] A. M. Trzynadlowski and E. Ritchie, "Comparative investigation of diagnosis media for induction motor: A case of rotor cage faults," *IEEE Trans. Ind. Electron.*, vol. 47, no. 5, pp. 1092–1099, Oct. 2000.

[12] R. Maier, "Protection of squirrel cage induction motor utilizing instantaneous power and phase information," *IEEE Trans. Ind. Appl.*, vol. 28, no. 2, pp. 376–380, Mar./Apr. 1992.

[13] M. Benbouzid, "A review of induction motors signature analysis as a medium for faults detection," *IEEE Trans. Ind. Electron.*, vol. 47, no. 5, pp. 984–993, Oct. 2000.

[14] M. Drif, N. Benouzza, and J. A. Dente, "Rotor cage detection in 3-phase induction motors using instantaneous power spectrum," in *Proc. Electrical Machines, Converters and Systems (ELECTRIMACS)*, Lisbon, Portugal, 1999, pp. 287–292.

[15] M. S. Bartlett, "Smoothing periodograms from time series with continuous spectra," *Nature (Lond.)*, vol. 161, pp. 686–687, May 1948.
[16] S. L. Marple, *Digital Spectral Analysis With Applications*. Englewood Cliffs, NJ: Prentice-Hall, 1987.
[17] G. Didier, H. Razik, O. Caspary, and E. Ternisien, "Rotor cage fault detection in induction motor using global modulation index on the instantaneous power spectrum," in *Proc. Symp. Diagnostics Electric Machines, Power Electronics and Drives (SDEMPED)*, Atlanta, GA, Aug. 2003, pp. 104–109.
[18] M. Haji and H. A. Toliyat, "Pattern recognition—A technique for induction machines rotor broken bar detections," *IEEE Trans. Energy Convers.*, vol. 16, no. 4, pp. 312–317, Dec. 2001.
[19] W. Deleroi, "Broken bar in squirrel-cage rotor of an induction motor—Part I: Description by superimposed fault-currents," *Arch. Elektrotech.*, vol. 67, pp. 91–99, 1984.
[20] G. Didier, "Modélisation et diagnostic de la machine asynchrone en présence de défaillances," Ph.D. dissertation, Univ. Henri Poincaré, Nancy, France, 2004.
[21] K. Kim, A. G. Parlos, and R. M. Bharadway, "Sensorless fault diagnosis of induction motors," *IEEE Trans. Ind. Electron.*, vol. 50, no. 5, pp. 1038–1051, Oct. 2003.

Gaëtan Didier was born in Saint-Dié, France, in 1978. He received the M.S. and Ph.D. degrees in electrical engineering from the Université Henri Poincaré, Nancy, France, in 2004.

He is currently an Assistant Professor at the Institut Universitaire de Technologie Henri Poincaré de Longwy and conducts research in the laboratory Groupe de Recherche en Electrotechnique et Electronique de Nancy. His main research interest concerns the diagnosis and modeling of induction motor under faults.

Eric Ternisien was born in Boulogne-sur-mer, France, in 1973. He received the M.S. and Ph.D. degrees in industrial systems engineering from the Université du Littoral, Côte d'Opale, France, in 2001.

In 2002, he joined the Université Henri Poincaré, Nancy, France, and the Centre de Recherche en Automatique de Nancy, as an Assistant Professor. His research fields concern the identification and localization of pollution sources, and since 2002, he has been working on the diagnostics of multiphase induction motors by signal processing techniques.

Olivier Caspary was born in Nantes, France, in 1966. He received the M.S. and Ph.D. degrees in electrical engineering from the Université Henri Poincaré, Nancy, France, in 1995.

Currently, he is an Assistant Professor at the Centre de Recherche en Automatique de Nancy, Nancy, France. His current research interests are in signal processing, source number estimation, and source separation.

Hubert Razik (M'98–SM'03) was born in Pompey, France, in 1962. He received the M.S. degree from the Ecole Normale Supérieure, Cachan, France, in 1987, the Ph.D. degree in electrical engineering from the Polytechnic Institute of Lorraine, Nancy, France, in 1991, and the "Habilitation à Diriger des Recherches" degree from the Université Henri Poincaré, Nancy, France, in 2000.

In 1993, he joined the Groupe de Recherche en Electrotechnique et Electronique de Nancy, Nancy, France, as an Assistant Professor. He is currently an Associate Professor of Electrical Engineering at the Institut Universitaire de Formation des Maîtres de Lorraine, Lorraine, France, and works at the Université Henri Poincaré, Nancy, France. He has authored or coauthored more than 60 scientific conference and journal papers. His fields of research deal with the modeling, the control and the diagnostic of multiphase induction motor.

Dr. Razik received the First-Prize Paper Award from the Electric Machines Committee at the 36th IEEE Industry Applications Society Annual Meeting, Chicago, IL, 2001. He is a member of the IEEE Industry Applications, IEEE Industrial Electronics, IEEE Power Electronics Society, and IEEE Power Engineering Societies.